MeCP2 controls dendritic morphogenesis via miR-199a-mediated Qki downregulation

Abbreviated Title: MeCP2/miR-199a/Qki axis promotes dendritic growth

Koichiro Irie[1,2], Hideyuki Nakashima[1], Masahiro Yamaguchi[3], Fumitaka Osakada[3], Norio Ozaki[4], Keita Tsujimura[4,5] and Kinichi Nakashima[1,*]

[1]Department of Stem Cell Biology and Medicine, Graduate School of Medical Sciences, Kyushu University, 3-1-1 Maidashi, Higashi-ku, Fukuoka, Fukuoka 812-8582, Japan

[2]Department of Neuroscience and Cell biology, Graduate School of Medicine, The University of Osaka, 2-2, Yamadaoka, Suita, Osaka, 565-0871, Japan

[3]Laboratory of Cellular Pharmacology, Department of Basic Medicinal Sciences, Graduate School of Pharmaceutical Sciences, Nagoya University, Furo, Chikusa, Nagoya, Aichi, 464-8601, Japan

[4]Department of Psychiatry, Graduate School of Medicine, Nagoya University, 65 Tsurumai, Showa-ku, Nagoya, Aichi, 466-8550, Japan

[5]Research Unit for Developmental Disorders, Institute of Advanced Research, Nagoya University, Furo, Chikusa-ku, Nagoya, Aichi, 464-8601, Japan

*Corresponding author: Kinichi Nakashima, Email: nakashima.kinichi.718@m.kyushu-u.ac.jp, TEL: +81-92-642-6195, FAX: +81-92-642-6561

Number of pages: 52

Number of figures, tables, multimedia, and 3D models: 8/0/0/0

Number of words for Abstract, Introduction, and Discussion: 211/774/1054

Abstract

Rett syndrome (RTT) (OMIM: 312750) is a severe neurodevelopmental disorder caused by mutations in the *MECP2* gene. Although decreased dendritic morphogenesis has been observed in the brain of RTT patients and mouse models, the molecular mechanisms underlying these dendritic anomalies remain unclear. We have previously shown that MeCP2 facilitates specific microRNA (miRNA) processing by associating with the miRNA microprocessor Drosha complex. In this study, we show that MeCP2 positively regulates dendritic formation via *miR-199a*, a specific target of the MeCP2-Drosha complex. Overexpression of MeCP2 and miR-199a promotes dendritic development such as increases in dendrite length, branching number, and complexity. In contrast, blocking miR-199a inhibited dendrite formation and abolished enhanced dendritic development induced by MeCP2 expression. We also demonstrate that the decreased dendrite outgrowth observed in MeCP2-deficient neurons could be rescued by miR-199a expression. In addition, we found that miR-199a targets the 3' untranslated region of *quaking (Qki)*, a negative regulator of dendritic development, and downregulates its protein expression level. Furthermore, we report an increase in the Qki

45 protein expression level in *miR-199a-2*-deficient brains and show that Qki knockdown

46 restores the dendritic morphology of *miR-199a-2*-Knockout (KO) neurons. Taken

47 together, these results suggest that the MeCP2/miR-199a/Qki axis is critical for proper

48 dendritic development and its dysregulation contributes to the dendritic pathology in RTT.

49

50 **Introduction**

51 Dendritic morphogenesis is critical for establishing functional neural circuits
52 during brain development (1, 2), with dendrite anomalies associated with
53 neurodevelopmental and neuropsychiatric disorders (3-5). Rett syndrome (RTT) is a
54 progressive neurodevelopmental disorder caused by loss-of-function mutations in the X-
55 linked *methyl-CpG binding protein 2 (MECP2)* gene (6). RTT patients develop normally
56 until 6-18 months of age, beyond which there is an onset of regression and various
57 neurological symptoms including seizures, stereotypies, loss of motor skills, autistic
58 features, and mental retardation (7, 8). Studies on postmortem brains have revealed
59 dendritic atrophy in RTT patients (9-11). Several mouse models lacking *Mecp2* (MeCP2-
60 KO) or carrying a mutation on *Mecp2* (12-16) mimic many RTT phenotypes including
61 motor impairments, seizures, and stereotypies (12, 13, 16). Reduced dendritic growth was
62 observed in these models (17, 18) and dendritic atrophy was reported in cultured MeCP2-
63 deficient neurons (19, 20). Therefore, impaired dendritic development may contribute to
64 RTT pathophysiology, with MeCP2 regulating dendritic formation. However, little is
65 known about the mechanisms underlying these phenomena.

66 MeCP2 belongs to the methylated DNA binding protein family and functions
67 as a transcriptional repressor by recruiting co-repressors including histone deacetylases
68 (HDACs) (21, 22), in addition to being a transcriptional activator and a splicing regulator
69 (23, 24).

70 MicroRNAs (miRNAs) are small noncoding RNAs that regulate gene
71 expression at the post-transcriptional level and are involved in many biological processes
72 including cell proliferation, differentiation, and development (25, 26). Primary miRNAs
73 (pri-miRNAs) are transcribed from DNA, processed into precursor miRNAs (pre-
74 miRNAs) by the nucleus-associated Drosha complex, and transported to the cytoplasm
75 by Exportin-5, where these are processed into mature miRNAs by Dicer. Mature miRNAs
76 bind to the 3' untranslated region (3'UTR) of target mRNAs and regulate gene expression
77 by inhibiting their translation or degradation (27, 28). Increasing evidence suggests a key
78 regulatory role of miRNAs in dendritic development. For example, miR-137 represses
79 dendritic morphogenesis by inhibiting Mind bomb 1 expression (29) and miR-9 regulates
80 dendritic formation by targeting the *repressor element-1 silencing transcription factor*
81 (*REST*) gene (30). Recently, we have shown that miR-214 positively controls dendritic

82 morphogenesis by regulating the expression of the schizophrenia-associated protein
83 quaking (Qki) (31).

84 We have reported that MeCP2 facilitates specific pri-miRNA processing by
85 associating with the Drosha complex and identified miR-199a as a target of the MeCP2-
86 Drosha complex (32). We also showed that miR-199a-5p, a mature form of miR-199a,
87 regulates mTOR signaling downstream of MeCP2 by inhibiting the expression of mTOR
88 signal inhibitors, and dysregulation of the MeCP2/miR-199a-5p/mTOR signaling
89 contributes to RTT neuronal phenotypes such as reduction in excitatory synaptic
90 transmission and density and smaller neuronal soma size (32). Furthermore, we
91 demonstrated that genetic deletion of miR-199a-2, a genomic loci of miR-199a,
92 recapitulates RTT phenotypes in mice and leads to decreased brain mTOR activity (32).
93 Although these findings identify miR-199a as a critical downstream target of MeCP2 in
94 RTT pathology, its contribution to dendritic phenotype remains unexplored. Despite
95 reports on suppression of dendritic development by MeCP2-mediated disruption of the
96 Drosha-DGCR8 complex (33), this negative regulation of dendritic morphology by
97 MeCP2 is inconsistent with the dendritic phenotype in postmortem brains of RTT

individuals and animal models (9-11, 17, 18).

In this study, both miR-199a-5p and miR-199a-3p were found to contribute to dendrite development downstream of MeCP2. Overexpression and inhibition of miR-199a in primary cultures of hippocampal neurons promoted and impeded dendrite development, respectively. Importantly, blocking miR-199a-3p strongly inhibited dendritic morphogenesis and completely abolished MeCP2-induced enhancement of dendritic growth, highlighting the crucial role of miR-199a-3p in dendritic development. We also demonstrated that miR-199a overexpression rescued dendritic impairment in MeCP2-KO neurons. Additionally, miR-199a-3p was observed to target *Qki* mRNA and suppress Qki expression. Indeed, Qki expression was elevated in miR-199a-2-KO mice brain and *Qki* knockdown improved impaired dendritic development in miR-199a-2-KO neurons. These results suggest that the MeCP2/miR-199a/Qki pathway plays a critical role in dendritic development and its dysregulation accounts for the dendritic phenotype in RTT mouse models.

115

116

117

118 **Results**

119 *Expression of MeCP2 correlates with mature-miR-199a production in developing*

120 *hippocampal neurons*

121 Although previous studies have shown that MeCP2 positively regulates

122 neuronal maturation (34, 35), little is known about the mechanistic basis of its regulation

123 of dendritic development. Previously, we have reported that MeCP2 promotes specific

124 miRNA processing and identified miR-199a as a MeCP2 target accountable for the RTT

125 phenotypes in mouse models of the disease (32). For this reason, we focused on the role

126 of miR-199a for understanding MeCP2-regulated dendritic development of neurons. To

127 explore the impact of the MeCP2/miR-199a pathway on dendritic morphogenesis, we

128 examined the expression patterns of MeCP2 and miR-199a in cultures of developing

129 hippocampal neurons. MeCP2 expression level gradually increased during neuronal

130 development (Fig. 1A and B). The pri-miR-199a is expressed from 2 gene loci, *miR-199a-*

131 *1* and *miR-199a-2*, and pre-miR-199a eventually generates 2 mature forms of miR-199a,

132 i.e., miR-199a-5p and miR-199a-3p, which are highly conserved across mammalian

133 species (Fig. 1C) (32). Expression levels of pri-miR-199a-1 and pri-miR-199a-2 in

134 cultured hippocampal neurons were found to increase at an early stage and then gradually
135 decrease at later stages of neuronal maturation (Fig. 1D and E), whereas that of the 2
136 types of mature miR-199a (miR-199a-5p and -3p) increased with neuronal dendrite
137 growth (Fig. 1F and G). These results imply that the MeCP2/miR-199a axis has a role in
138 the regulation of dendritic morphogenesis.
139
140 *MeCP2 and miR-199a promote dendritic development in cultured hippocampal neurons*
141 To investigate the influence of the MeCP2/miR-199a axis in the dendritic
142 development of neurons, we expressed MeCP2 or miR-199a in primary cultured
143 hippocampal neurons by infecting with lentiviral systems expressing GFP as control,
144 along with MeCP2 or miR-199a (Fig. 2A). Then, we evaluated dendritic morphology by
145 immunocytochemical assays utilizing antibodies against MAP2, a marker for neuronal
146 dendrites. In neurons expressing exogenous MeCP2, total dendrite length and branch
147 number were found to be significantly higher than that in control. Interestingly, we found
148 that miR-199a expression in neurons significantly increased dendrite length and branch
149 number to the same level as in MeCP2-expressing cells (Fig. 2B-D). We also performed

150 Sholl analysis by measuring the number of dendrites that cross concentric circles at
151 different radial distances from the cell body. The Sholl analysis revealed that miR-199a,
152 as well as MeCP2, enhances dendritic arborization compared to the control (Fig. 2E).
153 Together, these results suggest that the MeCP2/miR-199a pathway promotes dendritic
154 morphogenesis in hippocampal neurons.
155
156 *Both mature forms of miR-199a are required for dendritic development in hippocampal*
157 *neurons*
158 The pre-miR-199a generates 2 types of mature miRNAs, miR-199a-5p and -3p.
159 We, therefore, investigated which of these 2 mature forms contributes to dendritic
160 morphogenesis of neurons. We expressed the miRNA inhibitor (sponge) against either
161 miR-199a-5p (miR-199a5pi) or miR-199a-3p (miR-199a-3pi) in primary cultured
162 hippocampal neurons (Fig. 3A) and evaluated the resultant dendrite morphology.
163 Blocking of endogenous miR-199a-5p was found to lead to decreased total dendrite
164 length, but not branch number, compared with control samples, whereas miR-199a-3p
165 inhibition decreased both (Fig. 3B-D). Furthermore, expression of both miR-199a-5pi

166 and miR-199a-3pi reduced dendritic complexity, although the effect of miR-199a-5pi was
167 less pronounced compared with that of miR-199a-3pi (Fig. 3E). These results suggest that
168 both mature forms of miR-199a can regulate dendritic development, although miR-199a-
169 3p plays a more crucial role than miR-199a-5p.
170
171 *miR-199a acts downstream of MeCP2 in the regulation of dendritic development*
172 Since MeCP2 is known to promote the processing of pri-miR-199a, we next
173 examined whether miR-199a functions downstream of MeCP2 in dendrite formation. We
174 expressed the inhibitors for the respective mature miR-199a, along with MeCP2, in
175 cultured hippocampal neurons and evaluated the resultant dendritic morphology (Fig. 4A).
176 Inhibition of miR-199a-5p decreased the MeCP2-mediated enhancement of total dendrite
177 length, but not branch number, in neurons compared with control, whereas blocking miR-
178 199a-3p reduced both (Fig. 4B-D). Moreover, although the effect of miR-199a-3pi was
179 stronger than that of miR-199a-5pi, we found that expression of both the mature forms
180 inhibited MeCP2-induced increase in dendritic arborization (Fig. 4E). These results
181 suggest that both forms of mature miR-199a act as regulatory factors downstream of

182 MeCP2 in dendritic development, although miR-199a-3p is more stringently involved in

183 this regulation.

184

185 *MeCP2 and miR-199a enhance dendritic development in vivo*

186 We next examined the effects of MeCP2 and miR-199a in dendritic

187 morphogenesis *in vivo* in the mouse brain. For this, we expressed MeCP2 and miR-199a

188 in WT mouse brains by *in utero* electroporation at E14.5 and analyzed neuronal

189 morphology at P10. Almost all the GFP-positive transfected neurons at this stage were

190 located in layer IV (31). When we co-expressed MeCP2 and GFP in the WT mouse brain,

191 electroporated neurons showed enhanced dendrite length and branching number

192 compared with that of control (Fig. 5A-D). Furthermore, co-expression of miR-199a and

193 GFP in these WT neurons significantly promoted increase in dendrite length and

194 branching number, such that the latter were comparable to those in MeCP2-expressing

195 neurons (Fig. 5A-D). We also performed Sholl analysis and found that expression of

196 MeCP2 and miR-199a facilitates dendritic complexity and increases it to levels similar to

197 that in control conditions (Fig. 5E). Taken together, these data suggest that the

198 MeCP2/miR-199a axis positively regulates dendritic development *in vivo*.

199

200 *Expression of miR-199a rescues dendritic impairment in MeCP2-deficient neurons in*

201 *vivo*

202 We next asked whether miR-199a expression could reverse the impairment of

203 dendritic morphogenesis in MeCP2-deficient neurons. To this end, we expressed miR-

204 199a in the MeCP2-KO mouse brain by *in utero* electroporation at E14.5 and analyzed

205 neuronal morphology at P10. When we expressed only GFP in the MeCP2-KO mouse

206 brain, electroporated neurons showed decreased dendrite length and branching number

207 compared with that in WT. By contrast, the expression of miR-199a in MeCP2-KO

208 neurons significantly reversed the reduced dendrite length and branching number to the

209 level of WT neurons (Fig. 6A-D). Furthermore, Sholl analysis revealed that miR-199a

210 expression restored the dendritic complexity to levels observed in MeCP2-KO neurons

211 (Fig. 6E). Together with the *in vitro* results, these insights support the notion that miR-

212 199a functions as a downstream regulator of MeCP2 in dendritic development *in vivo*.

213

214 *miR-199a-3p targets 3'UTR of Qki mRNA and suppresses its protein expression in*

215 *neurons*

216 To understand the mechanisms by which miR-199a regulates dendritic

217 morphogenesis downstream of MeCP2, we attempted to identify genes targeted by each

218 mature form of miR-199a. We have previously demonstrated that miR-199a-5p positively

219 regulates mTOR signaling by targeting *Pde4d*, *Sirt1*, and *Hif1a* in hippocampal neurons

220 (32). Since mTOR signaling is known to promote morphological development of

221 dendrites (36), we reasoned that miR-199a-5p enhances dendritic arborization through

222 mTOR signaling. Additionally, since we have earlier shown that miR-199a-3p regulates

223 dendritic development to a greater extent compared with miR-199a-5p, we particularly

224 focused on identifying the genes targeted by miR-199a-3p. To this end, we first utilized

225 public databases such as miRDB (http://mirdb.org), TargetScan

226 (http://www.targetscan.org/vert_72/), and PicTar (https://pictar.mdc-berlin.de), and

227 identified 9 candidate target genes which were common in results from the three databases.

228 These included *amyloid beta (A4) precursor-like protein 2 (APLP2), Cbp/p300-*

229 *interacting transactivator, with Glu/Asp-rich carboxy-terminal domain, 2 (Cited2), F-box*

230 *and WD-40 domain protein 11 (Fbxw11), far upstream element (FUSE) binding protein*

231 *1 (Fubp1), mitogen-activated protein kinase kinase kinase 4 (Map3k4), muscleblind-like*

232 *1 (Mbnl1), platelet-derived growth factor receptor (Pdgfr), protein phosphatase 2*

233 *regulatory subunit B' epsilon (Ppp2r5e), and quaking (Qki)* (Fig. 7A). Since the 3'UTR

234 of *Qki* mRNA has the largest number of seed sites among these candidates and we have

235 recently shown that Qki negatively regulates dendritic development (31), we chose the

236 *Qki* gene as the most plausible target of miR-199a-3p. Next, to investigate whether miR-

237 199a-3p directly targets the *Qki* mRNA, we performed a luciferase reporter assay using

238 reporter constructs in which a luciferase reporter gene was placed under post-

239 transcriptional control of the native *Qki* 3'UTR or a *Qki* 3'UTR harboring mutations in

240 all three miR-199a-3p seed sites (Fig. 7B). These luciferase constructs, along with a miR-

241 199a-expressing plasmid, were co-transfected in hippocampal neurons, and luciferase

242 activity was measured. The latter showed significant decrease on miR-199a expression in

243 neurons containing the construct harboring all three native seed sequences. However, the

244 luciferase activities of reporter constructs with mutation in either of the three seed

245 sequences did not show such sensitivity to miR-199a expression (Fig. 7C). To determine

246 whether miR-199a-3p regulates Qki expression at the protein level, we expressed miR-
247 199a in hippocampal neurons and carried out immunoblotting assays using an anti-Qki
248 antibody. The *Qki* gene is known to generate three isoforms of the Qki protein (Qki-5,
249 Qki-6, and Qki-7) by alternative splicing (37). We found that the expression levels of all
250 three Qki isoforms were substantially decreased in miR-199a-expressing cells compared
251 with that in control cells (Fig. 7D and E). These findings suggest that miR-199a-3p
252 suppresses Qki protein expression in hippocampal neurons through interaction with the
253 3'UTR of *Qki* mRNA.
254
255 *miR-199a-2-KO neurons show reduced dendritic formation and Qki knockdown*
256 *reinstates abnormal dendritic morphology in miR-199a-2-deficient neurons*
257 We have previously generated miR-199a-2 deficient (miR-199a-2-KO) mice,
258 which recapitulates many RTT phenotypes such as reduction in body weight, brain size,
259 and neuronal soma size (32). We, therefore, attempted to confirm that miR-199a-3p
260 regulates Qki expression using the miR-199a-2-KO mouse model by estimating the
261 expression levels of miR-199a and Qki in miR-199a-2-KO neurons. Although miR-199a

262 is supposed to be expressed from 2 gene loci, expression levels of miR-199a-5p and miR-
263 199a-3p in the cortex of miR-199a-2 KO mice were significantly reduced compared with
264 those in WT mice (Fig. 8A). On the contrary, the expression of Qki protein was increased
265 in the same mice (Fig. 8B and C). Then, we investigated the dendritic morphology of
266 miR-199a-2 KO neurons and found that cultured hippocampal neurons from miR-199a-
267 2 KO mice exhibits decreased dendrite length and branching number compared with
268 neurons from WT mice. Further, we investigated whether downregulation of Qki
269 expression could reverse the dendritic phenotypes of miR-199a-2 KO neurons. For this,
270 we transfected miR-199a-2 KO neurons with lentivirus expressing shRNAs against *Qki*
271 and evaluated the resultant dendritic morphology. Interestingly, expression of shRNA
272 against *Qki* in miR-199a-2 KO neurons significantly restored the decrease in dendrite
273 length and branch number (Fig. 8D-F). Decreased dendritic complexity of miR-199a-2
274 KO neurons was also improved by Qki knockdown (Fig. 8G). From these results, we
275 concluded that miR-199a controls dendrite morphogenesis by targeting Qki.
276

277 **Discussion**

278 Although Rett syndrome is known to be caused by loss-of-function mutations
279 in the *MECP2* gene, the mechanisms by which dysfunction of *MECP2* leads to this
280 disease phenotype has remained largely elusive. A number of studies have reported
281 abnormal reductions in dendritic development in the postmortem brains of RTT
282 individuals and genetically engineered mouse models (9-11, 14, 17, 18, 34, 35).
283 Additionally, MeCP2-deficient neurons are known to exhibit abnormally decreased
284 dendritic development in *in vitro* culture systems (19, 20). Dendritic atrophy found in the
285 brain of RTT patients and mouse models of the disease have been related to dysfunctions
286 of the neural circuits (3). Therefore, these findings imply that defects in dendritic
287 morphology are a key feature in understanding RTT pathogenesis. However, the
288 molecular basis linking MeCP2 functions to the regulation of dendritic development is
289 still unclear. In this study, we have demonstrated the functional role of miR-199a in the
290 MeCP2-mediated regulation of dendritic morphogenesis. We first showed that the
291 expression of MeCP2 correlates with that of miR-199a in developing hippocampal
292 neurons. Transient up-regulation of pri-miR-199a expression was observed at early

293 developmental stages of these cultured hippocampal neurons, along with a reduction in
294 its expression at later stages. On the contrary, the expression levels of both MeCP2 and
295 mature miR-199a were upregulated during maturation of hippocampal neurons. These
296 observations led us to hypothesize that miR-199a has a critical role downstream of
297 MeCP2 in dendritic maturation and implied that the expression of mature miR-199a is
298 tightly regulated at the posttranscriptional level during neuronal maturation. Since we
299 have previously shown that miR-199a regulates multiple aspects of neurons, such as
300 neuronal growth and excitatory synaptic transmission and formation downstream of
301 MeCP2 (32), we postulated that miR-199a could also contribute to dendritic development
302 downstream of MeCP2. In support of our idea, we showed here that miR-199a positively
303 regulates morphological development of neuronal dendrites. Additionally, blocking of
304 mature miR-199a function was shown to abolish the MeCP2-mediated increase in
305 dendritic outgrowth. The expression of miR-199a in MeCP2-KO neurons was found to
306 improve the loss in dendritic morphology elicited by MeCP2 deficiency. In the present
307 study, we also investigated dendritic morphology of miR-199a-2 KO neurons and found
308 that dendrite formation was significantly decreased compared with WT, similar to that

309 observed in MeCP2 KO neurons. Since miR-199a-2 KO mice mimics various phenotypes
310 of MeCP2 KO mice (32), miR-199a KO neurons understandably recapitulated the
311 dendritic phenotype of MeCP2 KO neurons. Taken together, these findings clearly
312 indicate that miR-199a acts downstream of MeCP2 in the regulation of dendrite
313 morphogenesis and support the notion that miR-199a is a critical downstream target of
314 MeCP2 in RTT pathogenesis (32).

315 We also highlighted the differential effects of mature miR-199a, miR-199a-5p,
316 and mir-199a-3p on dendritic development. Whereas inhibition of miR-199a-5p reduced
317 only dendrite length, blocking miR-199a-3p induced a decrease in both dendrite length
318 and branch number. These results suggested that both mature forms of miR-199a regulate
319 dendrite formation through independent cascades by targeting different downstream
320 targets. We have earlier demonstrated that miR-199a-5p positively regulates neuronal
321 functions including neuronal growth, excitatory synaptic transmission, and
322 synaptogenesis by controlling mTOR signaling, and mTOR signaling has been reported
323 to enhance dendrite outgrowth (32, 36). Based on this, we postulated that miR-199a-5p
324 promotes dendritic formation, at least in part, by regulating mTOR signaling. On the

325 contrary, the target genes of miR-199a-3p in neurons have not been investigated so far.
326 Since *Qki* mRNA has three seed sequences of miR-199a-3p in its 3'UTR and we recently
327 reported the negative regulation of dendrite development by Qki (31), we hypothesized
328 that miR-199a-3p targets *Qki* gene in neurons. Our findings were in overall agreement
329 with the hypothesis and demonstrated that miR-199a-3p directly targets the 3'UTR of *Qki*
330 mRNA and suppresses Qki protein expression in neurons.

331 In the present study, the mechanisms underlying Qki-mediated regulation of
332 dendritic development remain to be determined. Qki is an RNA-binding protein that
333 belongs to the signal transduction and activation of RNA (STAR) protein family and is
334 reported to regulate RNA splicing, RNA export, RNA stability, and protein translation
335 (38, 39). A previous study has reported that Qki regulates the stability of actin-interacting
336 protein 1 (AIP1) mRNA during oligodendrocyte differentiation (40). Parallelly, a number
337 of studies have revealed that actin cytoskeleton dynamics plays an important role in the
338 regulation of dendritic morphogenesis (41, 42). Therefore, it is possible that Qki regulates
339 dendritic formation by targeting AIP1. Many other target mRNA candidates of Qki have
340 also been identified by SELEX (systematic evolution of ligands by exponential

341 enrichment) and bioinformatics based analysis (43). Intriguingly, *Tbr1*, *Wnt2a*, and
342 *Rab5a* have been identified as putative targets of Qki. A recent work has reported that
343 Tbr1 regulates laminar patterning of retinal ganglion cell dendrites (44). Another study
344 has shown that the Wnt/Dishevelled pathway controls development of dendritic
345 morphology and a component of the early endocytic pathway, Rab5a, enhances dendritic
346 morphogenesis of fly dendritic arborization neurons (45).

347 Genetic studies have implicated *Qki* in psychiatric disorders including
348 schizophrenia (46, 47), and mutations in *MECP2* have been reported in schizophrenia
349 patients (48). Given the dual lines of evidence on the contribution of altered dendritic
350 morphology in various neurological diseases (5, 49, 50) and MeCP2-mediated regulation
351 of Qki expression, it is possible that dysfunction of MeCP2/miR-199a/Qki axis
352 contributes to abnormal dendritic phenotypes associated with a variety of neurological
353 disorders.

354 Although an abnormal decrease in dendritic development is observed in the
355 postmortem brains of RTT patients and mouse models, the mechanisms underlying this
356 dendritic phenotype have not been understood to date. Our findings reveal a key role of

357 the MeCP2/miR-199a/Qki pathway in the regulation of dendritic morphogenesis and

358 provide a molecular basis linking MeCP2 dysfunction with impaired dendritic

359 development. We, therefore, propose that controlling this molecular pathway offers a new

360 avenue for the development of an effective therapeutic strategy for RTT.

361

362 **Material and Methods**

363 *Animals* – All aspects of animal care and treatment were carried out according
364 to the guidelines of the Experimental Animal Care and Use Committee of Kyushu
365 University and Nagoya University, respectively. Timed-pregnant ICR mice (Japan SLC,
366 Shizuoka, Japan) were used for the present research. The *Mecp2* mutant (*Mecp2*$^{tm1.1Jae}$)
367 used in this study was created by deleting exon 3 containing the methyl-DNA-binding
368 domain of MeCP2 (12) and was obtained from Jackson Laboratories. miR-199a-2-KO
369 mice (Acc. No.: CDB1185K; http://www2.clst.riken.jp/arg/micelist.html) were generated
370 as described previously (32). All mutant mice were maintained on a C57BL/6J (Jackson
371 Laboratories) or ICR (Japan SLC) background.

372 *Cell culture* – Hippocampal neuronal cultures were carried out as previously
373 described (51). Briefly, hippocampi were dissected from embryonic day 17.5 (E17.5)
374 mice and were digested in S-MEM (Gibco) containing 0.1% papain (Sigma), and
375 triturated with 60 mg/ml DNase I (Sigma) and 10% fetal bovine serum (FBS). Dissociated
376 cells were plated on poly-*L*-lysine (10 μg/ml, Sigma)-coated culture dishes at densities of
377 1×10^4 cells/cm^2 and 5×10^4 cells/cm^2 for immunocytochemical and immunoblotting

378 assays, respectively. Once neurons had adhered (after 3-4 h), the medium was replaced
379 with serum-free neuronal maintenance medium, comprising Neurobasal medium
380 (Invitrogen) supplemented with B-27 (Invitrogen) and 0.5 mM GlutaMAX (Invitrogen).
381 Cytosine β-D-arabinofuranoside hydrochloride (Sigma) was added 1 day after plating to
382 prevent the proliferation of undifferentiated and glial cells. The medium was changed
383 every 3 days. HEK 293T cells were cultured in DMEM containing 10% FBS and
384 gentamicin (Nacalai Tesque).

385 *Construction of vectors* – Lentiviral vectors used to express the short hairpin
386 RNA (shRNA) for *Qki* (pLLX-shQki) and FLAG-tagged Qki (pLEMPRA-Qki and
387 pLEMPRA-Qki-3'UTR) were generously provided by Drs. Z. Zhou and M. E. Greenberg.
388 pLLX and pLEMPRA are dual-promoter lentivirus vectors constructed by inserting the
389 U6 promoter-driven shRNA cassette 5' into the ubiquitin-C promoter in the FUIGW
390 plasmid (52, 53). The pLLX-primary-miR-199a plasmid was constructed by inserting a
391 PCR-amplified fragment from mouse genomic DNA into the HpaI and XhoI restriction
392 sites of pLLX. The shRNA for Qki and sponges against miR-199a-5p- or miR-199a-3p-
393 expressing lentivirus plasmids were constructed by inserting the following

394 oligonucleotides into the HpaI and XhoI sites of pLLX: sh-Qki-3-Fw, 5'-
395 TGGACTTACAGCTAAACAACTTTTCAAGAGAAAGTTGTTTAGCTGTAAGTCC
396 TTTTTTTGAAC-3', and sh-Qki-3-Rv, 5'-
397 tcgagttccaaaaaaGGACTTACAGCTAAACAACTTt-
398 ctcttgaaAAGTTGTTTAGCTGTAAGTCCa-3'; sponge-miR-199a-5p-Fw, 5'-
399 gacgttaacGAACAGGTACGTCTAACACTGGGGAACAGGTACGTCTAACACTGGG
400 GAACAGGTACGTCTAACACTGGGtttttttctcgaggtc, and sponge-miR-199a–5p-Rv; 5'-
401 gacctcgagaaaaaaCCCAGTGTTAGACGTACCTGTTCCCCAGTGTTAGACGTACCTG
402 TTCCCCAGTGTTAGACGTACCTGTTCgttaacgtc-3'; sponge-miR-199a-3p-Fw, and
403 5'-
404 gacgttaacTAACCAATGCATCGACTACTATTAACCAATGCATCGACTACTATTAAC
405 CAATGCATCGACTACTATtttttttctcgaggtc-3'; and sponge-miR-199a-3p-Rv and 5'-
406 gacctcgagaaaaaaATAGTAGTCGATGCATTGGTTAATAGTAGTCGATGCATTGGTTA
407 ATAGTAGTCGATGCATTGGTTAgttaacgtC-3'. *Qki*, cDNA fragments and its 3'UTR-
408 containing fragments were amplified by PCR using KOD polymerase (Toyobo) and
409 subsequently cloned into the EcoRI and AscI sites of pLEMPRA-MeCP2 (53). The

410 luciferase reporter plasmids pmirGLO-Qki-3'UTR-1ss-nat, -2ss-nat, and -3ss-nat were
411 constructed by inserting the genomic DNA fragments of Qki 3'UTR (1ss, +1361 to
412 +2374; 2ss, +3330 to +4337; and 3ss, +4134 to +5144) into the PmeI and XhoI sites of
413 pmir-GLO (Promega). Each of the mutated luciferase reporter constructs was obtained
414 by inserting the mutated 3'UTR of Qki with the seed regions of miR-199a-3p into the
415 PmeI and XhoI sites of pmir-GLO.

416 *In utero electroporation* – To investigate dendritic growth *in vivo*, *in utero*
417 electroporation was performed on WT or MeCP2-KO E14 mice (ICR background)
418 embryos, as described previously (54). Briefly, plasmid DNA (0.1 μg/μL in phosphate-
419 buffered saline (PBS) containing 0.1% Fast Green FCF dye) was injected (0.5-1 μl) into
420 the lateral ventricle of the embryonic brain from outside the uterus with a glass
421 micropipette (GD-1, Narishige). While holding the embryo in the uterus with forceps-
422 type electrodes (Nepa Gene), 50-ms electric pulses of 45 V each were delivered 5 times
423 at intervals of 950 ms using a CUY21 Single Cell Electroporator (Nepa Gene). Glass
424 micropipettes were prepared using a P-1000IVF micropipette puller (Sutter). Animals
425 were perfused with 4% paraformaldehyde at postnatal day 10 (P10). Collected brains

426 were postfixed with 4% paraformaldehyde overnight at 4°C and then equilibrated in 30%
427 sucrose. Brains were frozen at -80°C after embedding in Tissue-Tek optimal cutting
428 temperature (OCT) compound (Sakura Finetek) and serially sectioned at 40-μm thickness.

429 *Immunocytochemical assays* – Cells were fixed at the indicated day(s) *in vitro*
430 (DIV) with 4% paraformaldehyde in PBS, washed with PBS, permeabilized, and blocked
431 with blocking buffer (3% FBS and 0.1% Triton X-100 in PBS) at room temperature (RT).
432 The cells were then incubated with the primary antibody solution at RT for 3 h. The cells
433 were then washed with PBS and further incubated with the secondary antibody solution
434 at RT for 1 h. After further washing with PBS, these were mounted on glass slides.

435 *Immunohistochemical assays* – Brain sections were washed with PBS,
436 permeabilized, and blocked with blocking buffer at RT. These sections were then
437 incubated with the primary antibody solution overnight at 4°C, washed with PBS, and
438 further incubated with the secondary antibody solution at RT for 2 h. These sections were
439 mounted on glass slides, after washing with PBS. Fluorescence images were acquired
440 using a Zeiss LSM 700 confocal microscope with a 20× objective lens. Z series of 20
441 images were taken at 1-μm intervals at a resolution of 1,024 × 1,024 pixels.

442 *Immunoblotting* – Cells were lysed with a buffer containing 0.5% Nonidet P-
443 40, 10 mM Tris-HCl, pH 7.5, 150 mM NaCl, and 1% protease inhibitor mixture (Nacalai
444 Tesque). Lysates were sonicated and centrifuged at 20,000x*g* for 15 min at 4°C. Total cell
445 lysates were subjected to SDS-PAGE and transferred to a PVDF transfer membrane (GE
446 Healthcare). The blots were blocked with 0.3% skim milk in TBST (50 mM Tris-HCl, pH
447 7.5, 150 mM NaCl, 0.1% Tween 20), incubated with a primary antibody, and washed
448 again with TBST. This was followed by incubation with a peroxidase-conjugated
449 secondary antibody. Immunoreactive bands were detected by enhanced
450 chemiluminescence using the ECL Prime Western Blotting Detection Reagent (GE
451 Healthcare).

452 *Antibodies* – For immunocytochemical and immunohistochemical assays, the
453 following primary antibodies were used: chicken anti-green fluorescent protein (GFP)
454 (1:1000; Aves Labs) and guinea pig anti-microtubule-associated protein 2 (MAP2)
455 (1:1000; Synaptic Systems) antibodies. The following secondary antibodies were used:
456 CF488A donkey anti-chicken IgY (IgG) (H + L) highly cross-adsorbed (1:500; Biotium)
457 and CF555 donkey anti-guinea pig IgG (H + L) highly cross-adsorbed (1:500; Biotium).

458 Nuclei were stained using bisbenzimide H 33258 fluorochrome trihydrochloride (Nacalai
459 Tesque).

460 For immunoblotting, the following primary antibodies were used: rabbit anti-
461 MeCP2 (1:500; Diagenode), rabbit anti-QKI (1:250; ProteinTech), rabbit anti-GAPDH
462 (1:1000; Cell Signaling Technology), and mouse anti-β-actin (1:1000; Cell Signaling
463 Technology). The following secondary antibodies were used: anti-mouse IgG, HRP-
464 linked whole antibody from sheep (1:5000; GE Healthcare) and anti-rabbit IgG, HRP-
465 linked whole antibody from donkey (1:5000; GE Healthcare).

466 *Luciferase reporter assay* – Hippocampal neurons were co-transfected with
467 control (pLLX) or miR-199a expression vectors and pmir-GLO-Qki-1ss-nat, pmir-GLO-
468 Qki-1ss-mut, pmir-GLO-Qki-2ss-nat, pmir-GLO-Qki-2ss-mut pmir-GLO-Qki-3ss-nat,
469 or pmir-GLO-Qki-3ss-mut using Lipofectamine 2000 (Life Technologies). After
470 transfection, the cells were incubated for 3 days, and lysed with a Reporter Lysis Buffer.
471 Luciferase activity of the lysates was measured with the Dual-Glo Luciferase Assay
472 System (Promega) according to the manufacturer's protocol. Firefly luciferase activities
473 were determined by three independent transfections and normalized by comparison with

474 the Renilla luciferase activities of the internal control.

475 *Morphological analysis of cultured hippocampal neurons* – For analysis of
476 dendrite development *in vitro*, hippocampal neurons were subjected to immunostaining
477 with antibodies against MAP2 and GFP at 6 DIV. Dendrites were defined as MAP2-
478 positive neurites. Sholl analysis and quantification of dendritic length and branch number
479 were performed using the ImageJ software. For Sholl analysis, concentric circles with
480 radii increasing in 10 μm increments were defined from the center of the cell body. The
481 number of MAP2-positive dendrites crossing each circle was then counted.

482 For *in vivo* dendrite analysis, brain sections were subjected to
483 immunohistochemical labeling with the anti-GFP antibody. Total dendritic length and
484 branch number of GFP-positive neurons in layer IV were measured using ImageJ. For
485 Sholl analysis, concentric circles with radii increasing in 10 μm incrementsQ were
486 defined from the center of the cell body. The number of GFP-positive dendrites crossing
487 each circle was counted. The total number of crossings for each cell was calculated as an
488 objective measurement of total dendritic complexity.

489 *Quantitative real time-polymerase chain reaction (qRT-PCR) assays* – qRT-

490 PCR analysis was performed to measure the expression levels of primary and mature
491 miRNAs, as described previously (55). In brief, total RNA was extracted with TRIzol
492 (Invitrogen) and subjected to reverse transcription with the SuperScript VILO cDNA
493 Synthesis Kit (Invitrogen) according to the manufacturer's protocol. qRT-PCR was
494 performed with the StepOne Real-Time PCR System (Applied Biosystems). To detect
495 primary and mature miRNAs, a TaqMan MicroRNA Assay kit (Applied Biosystems) was
496 used in accordance with the manufacturer's protocol. Data analysis was performed using
497 the comparative Ct method. Results were normalized to the *Gapdh* or *U6* snRNA.

498 *Statistical analysis* – The results presented are the average of at least three
499 experiments, each performed in triplicates, with standard errors. Statistical analyses were
500 performed by one-way ANOVA, followed by Tukey's multiple comparison tests or by
501 Student's *t*-test, as appropriate, using Prism 5 (GraphPad software). Probabilities of $p <$
502 0.05 were considered significant.

503

504 **Acknowledgments:**

505 This work was funded by the Japan Society for the Promotion of Science (JSPS)
506 KAKENHI (24240051, 17H01390, and 16H06279 (PAGS)), and Intramural Research

507 Grants (27-7 and 30-9) for Neurological and Psychiatric Disorders of NCNP to K.N.,
508 Grant-in-Aid for Scientific Research on Innovative Areas (16H06527) to K.N.,
509 MEXT/JSPS KAKENHI Grant-in Scientific Research on Innovation Areas "Constructive
510 understanding of multi-scale dynamism of neuropsychiatric disorders" (19H05211) to
511 K.T., JSPS KAKENHI (18K06484) to K.T., JSPS KAKENHI (16K18391) to K.T., JSPS
512 KAKENHI (19K16918) to H.N. a grant from Kawano Masanori Memorial Public Interest
513 Incorporated Foundation for Promotion of Pediatrics (29-11) to K.T., and a NPO Rett
514 syndrome support organization grant (2019-01-09) to K.T. and (2019-02-10) to H.N. This
515 research was also supported by the Japan Agency for Medical Research and Development
516 (AMED) under Grant Number JP19ek0109411 to K.T., JP19dm0207075h to N.O.

517 We thank M.E. Greenberg and Z. Zhou for sharing reagents and all members of
518 the Laboratory of Molecular Neuroscience, Department of Stem Cell Biology and
519 Medicine, Kyushu University and Department of Psychiatry, Nagoya University. We
520 acknowledge technical assistance from the Research Support Center, Research Center for
521 Human Disease Modeling, Kyushu University Graduate School of Medical Science. We
522 also thank Yuko Masuda for technical assistance. We would like to thank Editage

(www.editage.com) for English language editing.

Conflict of Interest Statement: The authors declare no competing financial interests.

Author Contributions:

K.I., K.N., and K.T. designed research; K.I., H.N., M.Y., and K.T. performed experiments; K.I., H.N., F.O., N.O., K.N., and K.T analyzed data; K.I., K.N., and K.T. wrote the manuscript. All authors reviewed the manuscript.

1 Spruston, N. (2008) Pyramidal neurons: dendritic structure and synaptic integration. *Nat Rev Neurosci*, **9**, 206-221.

2 Craig, A.M. and Banker, G. (1994) Neuronal polarity. *Annu Rev Neurosci*, **17**, 267-310.

3 Kaufmann, W.E. and Moser, H.W. (2000) Dendritic anomalies in disorders associated with mental retardation. *Cereb Cortex*, **10**, 981-991.

4 Ramocki, M.B. and Zoghbi, H.Y. (2008) Failure of neuronal homeostasis results in common neuropsychiatric phenotypes. *Nature*, **455**, 912-918.

5 Rosoklija, G., Toomayan, G., Ellis, S.P., Keilp, J., Mann, J.J., Latov, N., Hays, A.P. and Dwork, A.J. (2000) Structural abnormalities of subicular dendrites in subjects with schizophrenia and mood disorders: preliminary findings. *Arch Gen Psychiatry*, **57**, 349-356.

6 Amir, R.E., Van den Veyver, I.B., Wan, M., Tran, C.Q., Francke, U. and Zoghbi, H.Y. (1999) Rett syndrome is caused by mutations in X-linked

547 MECP2, encoding methyl-CpG-binding protein 2. *Nat Genet*, **23**, 185-188.
548 7 Hagberg, B., Aicardi, J., Dias, K. and Ramos, O. (1983) A progressive
549 syndrome of autism, dementia, ataxia, and loss of purposeful hand use in
550 girls: Rett's syndrome: report of 35 cases. *Ann Neurol*, **14**, 471-479.
551 8 Rett, A. (1966) [On a unusual brain atrophy syndrome in
552 hyperammonemia in childhood]. *Wien Med Wochenschr*, **116**, 723-726.
553 9 Armstrong, D., Dunn, J.K., Antalffy, B. and Trivedi, R. (1995)
554 Selective dendritic alterations in the cortex of Rett syndrome. *J Neuropathol*
555 *Exp Neurol*, **54**, 195-201.
556 10 Belichenko, P.V., Oldfors, A., Hagberg, B. and Dahlstrom, A. (1994)
557 Rett syndrome: 3-D confocal microscopy of cortical pyramidal dendrites and
558 afferents. *Neuroreport*, **5**, 1509-1513.
559 11 Kaufmann, W.E., MacDonald, S.M. and Altamura, C.R. (2000)
560 Dendritic cytoskeletal protein expression in mental retardation: an
561 immunohistochemical study of the neocortex in Rett syndrome. *Cereb Cortex*,
562 **10**, 992-1004.
563 12 Chen, R.Z., Akbarian, S., Tudor, M. and Jaenisch, R. (2001)
564 Deficiency of methyl-CpG binding protein-2 in CNS neurons results in a Rett-
565 like phenotype in mice. *Nat Genet*, **27**, 327-331.
566 13 Guy, J., Hendrich, B., Holmes, M., Martin, J.E. and Bird, A. (2001) A
567 mouse Mecp2-null mutation causes neurological symptoms that mimic Rett
568 syndrome. *Nat Genet*, **27**, 322-326.
569 14 Jentarra, G.M., Olfers, S.L., Rice, S.G., Srivastava, N., Homanics,
570 G.E., Blue, M., Naidu, S. and Narayanan, V. (2010) Abnormalities of cell
571 packing density and dendritic complexity in the MeCP2 A140V mouse model
572 of Rett syndrome/X-linked mental retardation. *BMC Neurosci*, **11**, 19.
573 15 Pitcher, M.R., Herrera, J.A., Buffington, S.A., Kochukov, M.Y.,
574 Merritt, J.K., Fisher, A.R., Schanen, N.C., Costa-Mattioli, M. and Neul, J.L.
575 (2015) Rett syndrome like phenotypes in the R255X Mecp2 mutant mouse are
576 rescued by MECP2 transgene. *Hum Mol Genet*, **24**, 2662-2672.
577 16 Shahbazian, M., Young, J., Yuva-Paylor, L., Spencer, C., Antalffy, B.,
578 Noebels, J., Armstrong, D., Paylor, R. and Zoghbi, H. (2002) Mice with
579 truncated MeCP2 recapitulate many Rett syndrome features and display

580 hyperacetylation of histone H3. *Neuron*, **35**, 243-254.
581 17 Fukuda, T., Itoh, M., Ichikawa, T., Washiyama, K. and Goto, Y. (2005)
582 Delayed maturation of neuronal architecture and synaptogenesis in cerebral
583 cortex of Mecp2-deficient mice. *J Neuropathol Exp Neurol*, **64**, 537-544.
584 18 Kishi, N. and Macklis, J.D. (2004) MECP2 is progressively expressed
585 in post-migratory neurons and is involved in neuronal maturation rather
586 than cell fate decisions. *Mol Cell Neurosci*, **27**, 306-321.
587 19 Larimore, J.L., Chapleau, C.A., Kudo, S., Theibert, A., Percy, A.K.
588 and Pozzo-Miller, L. (2009) Bdnf overexpression in hippocampal neurons
589 prevents dendritic atrophy caused by Rett-associated MECP2 mutations.
590 *Neurobiol Dis*, **34**, 199-211.
591 20 Nerli, E., Roggero, O.M., Baj, G. and Tongiorgi, E. (2020) In vitro
592 modeling of dendritic atrophy in Rett syndrome: determinants for phenotypic
593 drug screening in neurodevelopmental disorders. *Sci Rep*, **10**, 2491.
594 21 Jones, P.L., Veenstra, G.J., Wade, P.A., Vermaak, D., Kass, S.U.,
595 Landsberger, N., Strouboulis, J. and Wolffe, A.P. (1998) Methylated DNA and
596 MeCP2 recruit histone deacetylase to repress transcription. *Nat Genet*, **19**,
597 187-191.
598 22 Nan, X., Ng, H.H., Johnson, C.A., Laherty, C.D., Turner, B.M.,
599 Eisenman, R.N. and Bird, A. (1998) Transcriptional repression by the methyl-
600 CpG-binding protein MeCP2 involves a histone deacetylase complex. *Nature*,
601 **393**, 386-389.
602 23 Chahrour, M., Jung, S.Y., Shaw, C., Zhou, X., Wong, S.T., Qin, J. and
603 Zoghbi, H.Y. (2008) MeCP2, a key contributor to neurological disease,
604 activates and represses transcription. *Science*, **320**, 1224-1229.
605 24 Young, J.I., Hong, E.P., Castle, J.C., Crespo-Barreto, J., Bowman,
606 A.B., Rose, M.F., Kang, D., Richman, R., Johnson, J.M., Berget, S. *et al.* (2005)
607 Regulation of RNA splicing by the methylation-dependent transcriptional
608 repressor methyl-CpG binding protein 2. *Proc Natl Acad Sci U S A*, **102**,
609 17551-17558.
610 25 Bartel, D.P. (2004) MicroRNAs: genomics, biogenesis, mechanism,
611 and function. *Cell*, **116**, 281-297.
612 26 Tufekci, K.U., Meuwissen, R.L. and Genc, S. (2014) The role of

613 microRNAs in biological processes. *Methods Mol Biol*, **1107**, 15-31.
614 27 Winter, J., Jung, S., Keller, S., Gregory, R.I. and Diederichs, S. (2009)
615 Many roads to maturity: microRNA biogenesis pathways and their regulation.
616 *Nat Cell Biol*, **11**, 228-234.
617 28 Siomi, H. and Siomi, M.C. (2010) Posttranscriptional regulation of
618 microRNA biogenesis in animals. *Mol Cell*, **38**, 323-332.
619 29 Smrt, R.D., Szulwach, K.E., Pfeiffer, R.L., Li, X., Guo, W., Pathania,
620 M., Teng, Z.Q., Luo, Y., Peng, J., Bordey, A. *et al.* (2010) MicroRNA miR-137
621 regulates neuronal maturation by targeting ubiquitin ligase mind bomb-1.
622 *Stem Cells*, **28**, 1060-1070.
623 30 Giusti, S.A., Vogl, A.M., Brockmann, M.M., Vercelli, C.A., Rein, M.L.,
624 Trumbach, D., Wurst, W., Cazalla, D., Stein, V., Deussing, J.M. *et al.* (2014)
625 MicroRNA-9 controls dendritic development by targeting REST. *Elife*, **3**.
626 31 Irie, K., Tsujimura, K., Nakashima, H. and Nakashima, K. (2016)
627 MicroRNA-214 Promotes Dendritic Development by Targeting the
628 Schizophrenia-associated Gene Quaking (Qki). *J Biol Chem*, **291**, 13891-
629 13904.
630 32 Tsujimura, K., Irie, K., Nakashima, H., Egashira, Y., Fukao, Y.,
631 Fujiwara, M., Itoh, M., Uesaka, M., Imamura, T., Nakahata, Y. *et al.* (2015)
632 miR-199a Links MeCP2 with mTOR Signaling and Its Dysregulation Leads
633 to Rett Syndrome Phenotypes. *Cell Rep*, **12**, 1887-1901.
634 33 Cheng, T.L., Wang, Z., Liao, Q., Zhu, Y., Zhou, W.H., Xu, W. and Qiu,
635 Z. (2014) MeCP2 suppresses nuclear microRNA processing and dendritic
636 growth by regulating the DGCR8/Drosha complex. *Dev Cell*, **28**, 547-560.
637 34 Chahrour, M. and Zoghbi, H.Y. (2007) The story of Rett syndrome:
638 from clinic to neurobiology. *Neuron*, **56**, 422-437.
639 35 Smrt, R.D., Eaves-Egenes, J., Barkho, B.Z., Santistevan, N.J., Zhao,
640 C., Aimone, J.B., Gage, F.H. and Zhao, X. (2007) Mecp2 deficiency leads to
641 delayed maturation and altered gene expression in hippocampal neurons.
642 *Neurobiol Dis*, **27**, 77-89.
643 36 Jaworski, J., Spangler, S., Seeburg, D.P., Hoogenraad, C.C. and
644 Sheng, M. (2005) Control of dendritic arborization by the phosphoinositide-3'-
645 kinase-Akt-mammalian target of rapamycin pathway. *J Neurosci*, **25**, 11300-

646 11312.
647 37 Ebersole, T.A., Chen, Q., Justice, M.J. and Artzt, K. (1996) The
648 quaking gene product necessary in embryogenesis and myelination combines
649 features of RNA binding and signal transduction proteins. *Nat Genet*, **12**,
650 260-265.
651 38 Hall, M.P., Nagel, R.J., Fagg, W.S., Shiue, L., Cline, M.S., Perriman,
652 R.J., Donohue, J.P. and Ares, M., Jr. (2013) Quaking and PTB control
653 overlapping splicing regulatory networks during muscle cell differentiation.
654 *RNA*, **19**, 627-638.
655 39 Larocque, D. and Richard, S. (2005) QUAKING KH domain proteins
656 as regulators of glial cell fate and myelination. *RNA Biol*, **2**, 37-40.
657 40 Doukhanine, E., Gavino, C., Haines, J.D., Almazan, G. and Richard,
658 S. (2010) The QKI-6 RNA binding protein regulates actin-interacting protein-
659 1 mRNA stability during oligodendrocyte differentiation. *Mol Biol Cell*, **21**,
660 3029-3040.
661 41 Coles, C.H. and Bradke, F. (2015) Coordinating neuronal actin-
662 microtubule dynamics. *Curr Biol*, **25**, R677-691.
663 42 Luo, L. (2002) Actin cytoskeleton regulation in neuronal
664 morphogenesis and structural plasticity. *Annu Rev Cell Dev Biol*, **18**, 601-635.
665 43 Galarneau, A. and Richard, S. (2005) Target RNA motif and target
666 mRNAs of the Quaking STAR protein. *Nat Struct Mol Biol*, **12**, 691-698.
667 44 Liu, J., Reggiani, J.D.S., Laboulaye, M.A., Pandey, S., Chen, B.,
668 Rubenstein, J.L.R., Krishnaswamy, A. and Sanes, J.R. (2018) Tbr1 instructs
669 laminar patterning of retinal ganglion cell dendrites. *Nat Neurosci*, **21**, 659-
670 670.
671 45 Jan, Y.N. and Jan, L.Y. (2010) Branching out: mechanisms of
672 dendritic arborization. *Nat Rev Neurosci*, **11**, 316-328.
673 46 Klempan, T.A., Ernst, C., Deleva, V., Labonte, B. and Turecki, G.
674 (2009) Characterization of QKI gene expression, genetics, and epigenetics in
675 suicide victims with major depressive disorder. *Biol Psychiatry*, **66**, 824-831.
676 47 Chenard, C.A. and Richard, S. (2008) New implications for the
677 QUAKING RNA binding protein in human disease. *J Neurosci Res*, **86**, 233-
678 242.

679 48 Shibayama, A., Cook, E.H., Feng, J., Glanzmann, C., Yan, J.,
680 Craddock, N., Jones, I.R., Goldman, D., Heston, L.L. and Sommer, S.S. (2004)
681 MECP2 structural and 3'-UTR variants in schizophrenia, autism and other
682 psychiatric diseases: a possible association with autism. *Am J Med Genet B*
683 *Neuropsychiatr Genet*, **128B**, 50-53.
684 49 Soetanto, A., Wilson, R.S., Talbot, K., Un, A., Schneider, J.A., Sobiesk,
685 M., Kelly, J., Leurgans, S., Bennett, D.A. and Arnold, S.E. (2010) Association
686 of anxiety and depression with microtubule-associated protein 2- and
687 synaptopodin-immunolabeled dendrite and spine densities in hippocampal
688 CA3 of older humans. *Arch Gen Psychiatry*, **67**, 448-457.
689 50 Kulkarni, V.A. and Firestein, B.L. (2012) The dendritic tree and
690 brain disorders. *Mol Cell Neurosci*, **50**, 10-20.
691 51 Kaech, S. and Banker, G. (2006) Culturing hippocampal neurons.
692 *Nat Protoc*, **1**, 2406-2415.
693 52 Lois, C., Hong, E.J., Pease, S., Brown, E.J. and Baltimore, D. (2002)
694 Germline transmission and tissue-specific expression of transgenes delivered
695 by lentiviral vectors. *Science*, **295**, 868-872.
696 53 Zhou, Z., Hong, E.J., Cohen, S., Zhao, W.N., Ho, H.Y., Schmidt, L.,
697 Chen, W.G., Lin, Y., Savner, E., Griffith, E.C. *et al.* (2006) Brain-specific
698 phosphorylation of MeCP2 regulates activity-dependent Bdnf transcription,
699 dendritic growth, and spine maturation. *Neuron*, **52**, 255-269.
700 54 Kawauchi, T., Sekine, K., Shikanai, M., Chihama, K., Tomita, K.,
701 Kubo, K., Nakajima, K., Nabeshima, Y. and Hoshino, M. (2010) Rab GTPases-
702 dependent endocytic pathways regulate neuronal migration and maturation
703 through N-cadherin trafficking. *Neuron*, **67**, 588-602.
704 55 Suzuki, H.I., Yamagata, K., Sugimoto, K., Iwamoto, T., Kato, S. and
705 Miyazono, K. (2009) Modulation of microRNA processing by p53. *Nature*, **460**,
706 529-533.

707

708 **Legends to Figures**:

709 **Fig. 1. Expression patterns of MeCP2 and miR-199a in hippocampal neurons during**

710 **development**

711 *A*, Expression levels of MeCP2 were measured by immunoblotting in cultures of

712 developing hippocampal neurons at 0, 1, 3, 6, and 10 days *in vitro* (DIV).

713 *B*, Quantification of MeCP2 expression in *A*.

714 *C*, Diagrammatic representation of the sequence of pre-miR-199a-1 and pre-miR-199a-2.

715 The nucleotide sequences of mature miR-199a-5p and miR-199a-3p are highly conserved

716 among several species. The regions highlighted in gray indicate the seed sequence.

717 *D* - *G*, Expression levels of primary miR-199a-1 (D), primary miR-199a-2 (E), mature

718 miR-199a-5p (F), and mature miR-199a-3p (G) were measured by qRT-PCR in cultures

719 of developing hippocampal neurons at 0, 1, 3, 6, and 10 DIV.

720

721 **Fig. 2. MeCP2 and miR-199a promote dendritic development of cultured**

722 **hippocampal neurons**

723 *A*, Diagrammatic representations of lentiviral vector constructs. GFP and MeCP2 are

724 expressed under the ubiquitin promoter. miR-199a is expressed as a short hairpin RNA

725 under the U6 RNA polymerase III promoter, and GFP is expressed under the ubiquitin

726 promoter.

727 *B*, Representative images of hippocampal neurons, labeled with anti-MAP2 (red) and

728 anti-GFP (green) antibodies at 6 days *in vitro* (DIV).

729 *C and D*, Quantification of total dendrite length (C) and dendrite branch number (D) in

730 *B*. Student's *t*-test, *, $p < 0.05$. n = 4 independent experiments; at least 50 neurons were

731 analyzed in each experiment.

732 *E*, quantification of dendrite complexity by Sholl analysis of neurons infected with

733 lentiviruses co-expressing MeCP2 and miR-199a at 6 DIV. Student's *t*-test, *, $p < 0.05$;

734 **, $p < 0.01$; ***, $p < 0.001$. Fifty neurons were analyzed at each condition.

735

736 **Fig. 3. Both mature forms of miR-199a are required for dendritic development in**

737 **hippocampal neurons**

738 *A*, diagrammatic representations of lentiviral vector constructs expressing sponges

739 against miR-199a-5p and miR-199a-3p. These sponges are expressed as a short hairpin

740 RNA under the U6 RNA polymerase III promoter, and GFP is expressed under the

741 ubiquitin promoter.

742 *B*, representative images of hippocampal neurons infected with lentivirus expressing

743 sponges against miR-199a-5p and miR-199a-3p. These neurons were labeled with anti-

744 MAP2 (red) and anti-GFP (green) antibodies at 6 days *in vitro* (DIV).

745 *C and D*, quantification of total dendrite length (C) and dendrite branch number (D) in *B*.

746 Student's *t*-test, ***, $p < 0.001$; n.s., not significant. n = 4 independent experiments; at

747 least 50 neurons were analyzed in each experiment.

748 *E*, quantification of dendrite complexity by Sholl analysis of neurons infected with

749 lentiviruses expressing sponges against miR-199a-5p and miR-199a-3p at 6 DIV.

750 Student's *t*-test, *, $p < 0.05$; **, $p < 0.01$. Fifty neurons were analyzed for each condition.

751

752 **Fig. 4. Inhibition of miR-199a counteracts the effect of MeCP2 expression in**

753 **hippocampal neurons**

754 *A*, diagrammatic representations of lentiviral vector constructs expressing MeCP2 and

755 sponges against miR-199a-5p or miR-199a-3p. These sponges are expressed as a short

756 hairpin under the U6 RNA polymerase III promoter, and GFP and MeCP2 are expressed

757 under the ubiquitin promoter.

758 *B*, representative images of hippocampal neurons infected with lentivirus expressing

759 MeCP2 and sponges against miR-199a-5p or miR-199a-3p. These neurons were labeled

760 with anti-MAP2 (red) and anti-GFP (green) antibodies at 6 DIV.

761 *C and D*, quantification of total dendrite length (C) and dendrite branch number (D) in *B*.

762 Student's *t*-test, *, $p < 0.05$; **, $p < 0.01$; ***, $p < 0.001$. n = 4 independent experiments;

763 at least 50 neurons were analyzed in each experiment.

764 *E*, quantification of dendrite complexity by Sholl analysis of neurons infected with

765 lentiviruses expressing MeCP2 and sponges against miR-199a-5p or miR-199a-3p at 6

766 DIV. Student's *t*-test, *, $p < 0.05$; **, $p < 0.01$; ***, $p < 0.001$. Fifty neurons were analyzed

767 for each condition.

768

769 **Fig. 5. MeCP2 and miR-199a promote dendritic development *in vivo***

770 *A*, representative image of a transfected brain section labeled with anti-GFP antibody. WT

771 mice embryos were transfected with plasmids expressing only GFP (control), or GFP

772 along with MeCP2 (MeCP2) or miR-199a (miR-199a) by *in utero electroporation* at E14

773 and sacrificed at P10. Scale bar, 50 μm.

774 *B*, representative tracing images of neurons transfected with the constructs described in

775 *A*. Scale bar, 50 μm.

776 *C and D*, quantification of total dendrite length (C) and dendrite branch number (D) in

777 *B*. One-way ANOVA, Tukey's post-hoc test, ***, $p < 0.001$. Number of cells analyzed:

778 control, 13 neurons from three brains; MeCP2, 14 neurons from three brains; miR-199a,

779 12 neurons from three brains.

780 *E*, quantification of dendrite complexity by Sholl analysis of neurons in *C*. One-way

781 ANOVA, Tukey's post-test, *, $p < 0.05$; **, $p < 0.01$; ***, $p < 0.001$.

782

783 **Fig. 6. Expression of miR-199a reverses dendritic impairment in MeCP2 knockout**

784 **neurons *in vivo***

785 *A*, Representative image of a transfected brain section labeled with anti-GFP antibody.

786 WT and MeCP2-KO mice embryos were transfected with plasmids expressing only GFP

787 (control), or GFP together with miR-199a (miR-199a) by *in utero electroporation* at E14

788 and sacrificed at P10. Scale bar, 50 μm.

789 *B*, Representative tracing images of neurons transfected with the constructs described in

790 *A*. Scale bar, 50 μm.

791 *C and D*, Quantification of total dendrite length (C) and dendrite branch number (D) in

792 *B*. One-way ANOVA, Tukey's post-test, *, $p < 0.05$; ***, $p < 0.001$. Number of cells

793 analyzed: WT + control, 19 neurons from three brains; MeCP2-KO + control, 17

794 neurons from three brains; MeCP2-KO + miR-199a, 16 neurons from three brains.

795 *E*, Quantification of dendrite complexity by Sholl analysis of neurons in *C*. One-way

796 ANOVA, Tukey's post-test, *, $p < 0.05$; **, $p < 0.01$; ***, $p < 0.001$.

797

798 **Fig. 7. miR-199a-3p targets *Qki* in hippocampal neurons**

799 *A*, Flow chart showing the screening process for selection of downstream targets of miR-

800 199a-3p.

801 *B*, Diagrammatic representations of luciferase reporter constructs that were inserted in a

802 part of the Qki 3'UTR DNA fragment including each seed site, showing the miR-199a-

803 3p sequence, and each miR-199a-3p target sequence of native type (nat) and its mutated

804 sequence (mut). The 5' seed sequences of miR-199a-3p are marked by blue boxes.

805 *C*, Luciferase activity of *Qki* 3'UTR was suppressed by miR-199a overexpression at 3

806 days after transfection (left). Student's *t*-test, *, $p < 0.05$; n.s., not significant. n = 3

807 independent experiments.

808 *D*, Western blotting analysis showing that the levels of all three isoforms of Qki protein

809 were decreased in hippocampal neurons infected with lentivirus vector constructs

810 expressing miR-199a at 6 days *in vitro* (DIV).

811 *E*, Quantification of total Qki protein level in *B*. Student's *t*-test, *, $p < 0.05$. n = 3

812 independent experiments.

813

814 **Fig. 8. miR-199a-deficient neurons show reduced dendrite formation and Qki**

815 **knockdown restores abnormal dendritic phenotype**

816 *A*, Expression levels of mature forms of miR-199a-5p and miR-199a-3p in miR-199a-2-

817 KO cortex at E17 by qRT-PCR assays.

818 *B*, Representative immunoblots of Qki, generated by immunoblotting with anti-Qki

819 antibody in miR-199a-2-KO mice cortex for estimation of Qki protein levels.

820 *C*, Quantification of Qki protein levels in *B*. Student's *t*-test, *, $p < 0.05$. n = 3 independent

821 experiments.

822 *D*, Representative images of cultured hippocampal neurons from miR-199a-2-KO mice

823 as indicated, infected with lentivirus vector constructs expressing shRNA against *Qki* and

824 labeled with anti-GFP (green) and anti-MAP2 (red) antibodies at 6 days *in vitro* (DIV).

825 *E and F*, Quantification of total dendrite length (E) and dendrite branch number (F) in *D*.

826 Student's *t*-test, *, $p < 0.05$; **, $p < 0.01$; ***, $p < 0.001$. n = 4 independent experiments;

827 at least 50 neurons were analyzed in each experiment. Scale bar, 50 μm.

828 *G*, Quantification of dendrite complexity by Sholl analysis of neurons from miR-199a-2-

829 KO mice infected with lentivirus vector constructs expressing shRNA against *Qki*.

830 Student's *t*-test, *, $p < 0.05$; **, $p < 0.01$; ***, $p < 0.001$. Fifty neurons were analyzed for

831 each condition.

K. Irie et al. Fig. 1

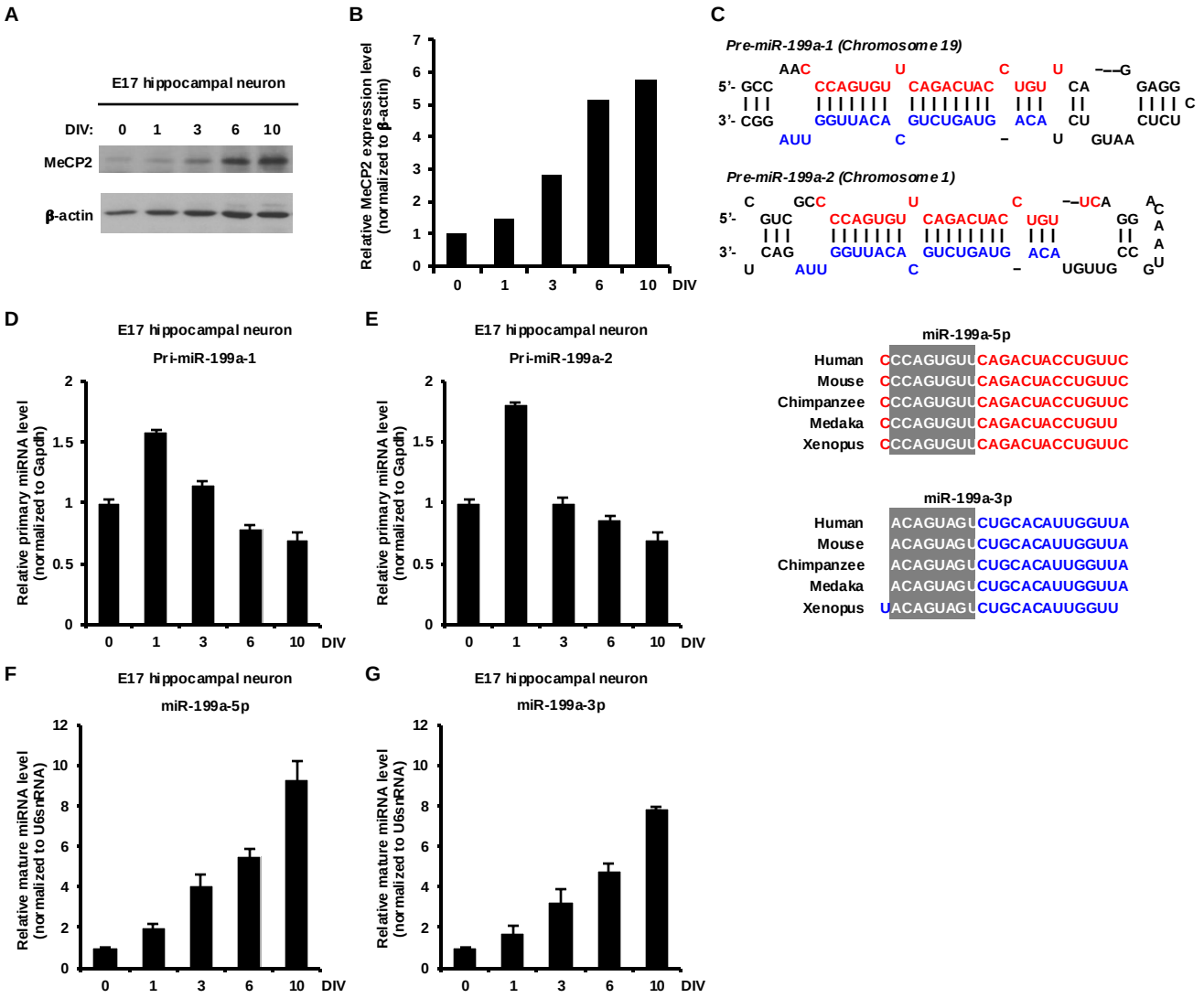

K. Irie et al. Fig. 2

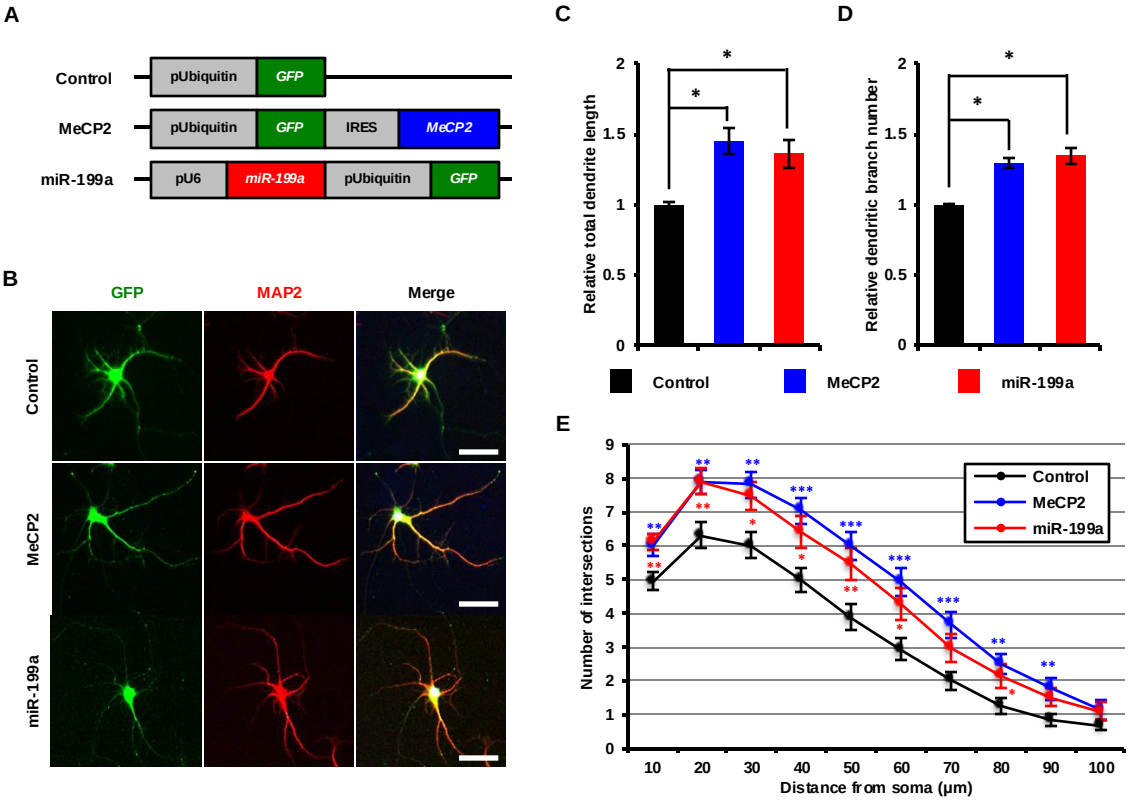

K. Irie et al. Fig. 3

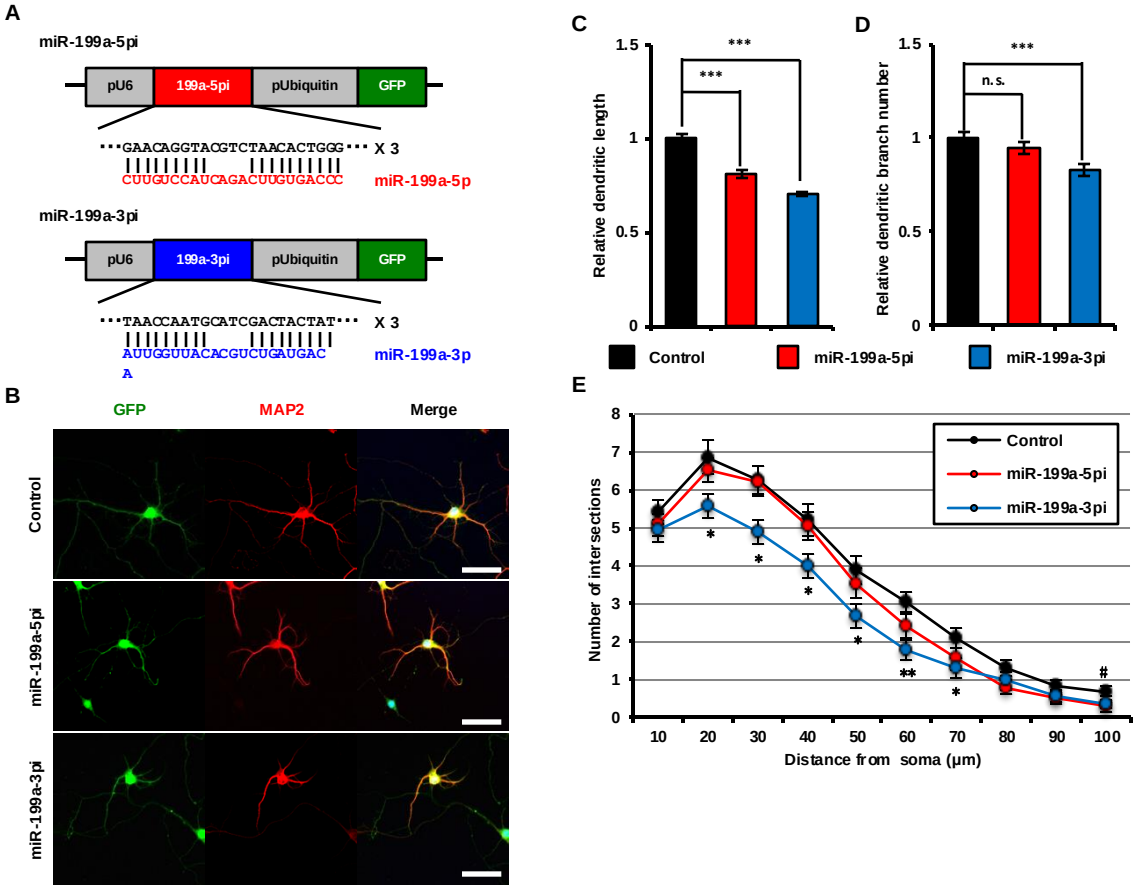

K. Irie et al. Fig. 4

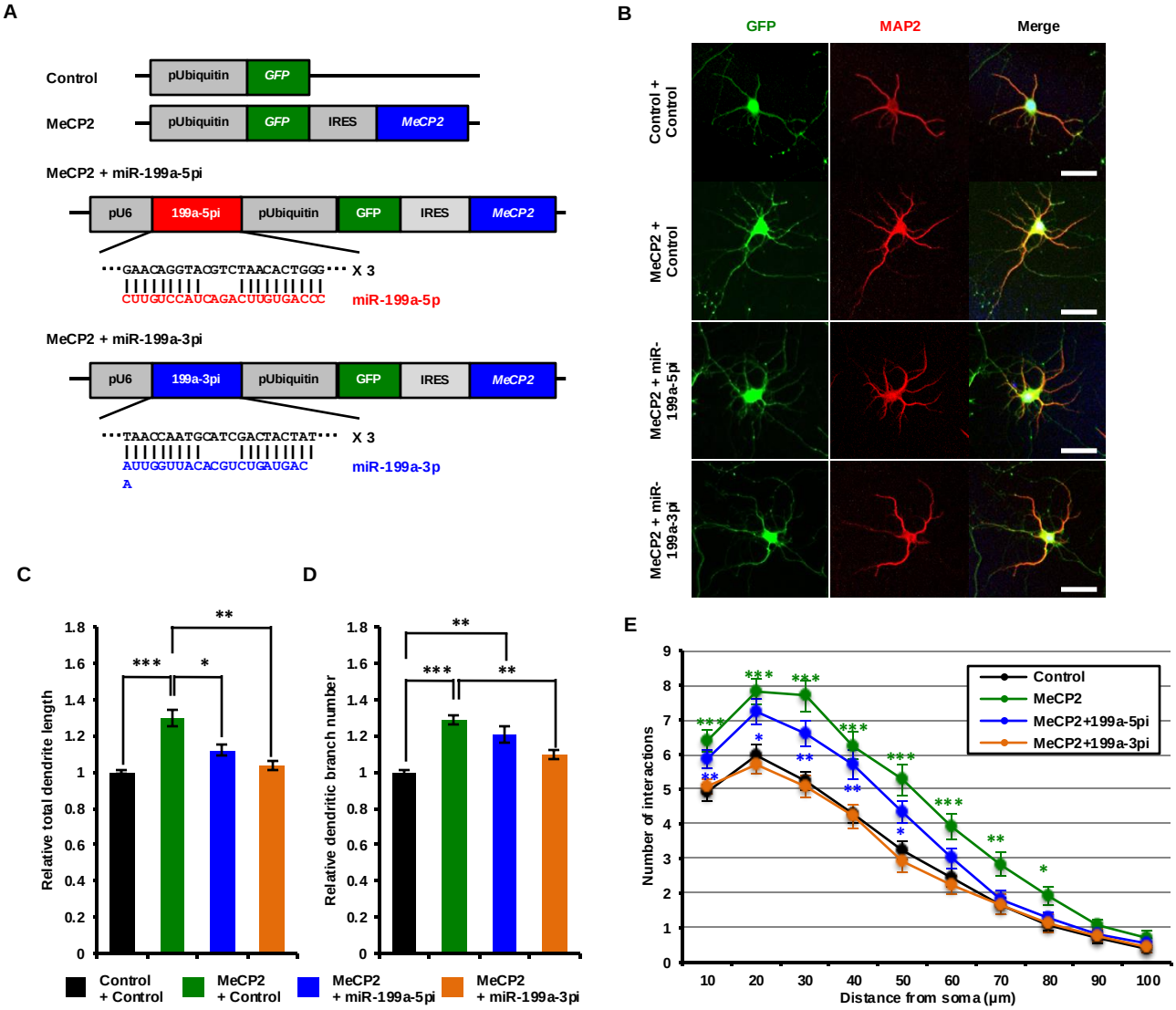

K. Irie et al. Fig. 5

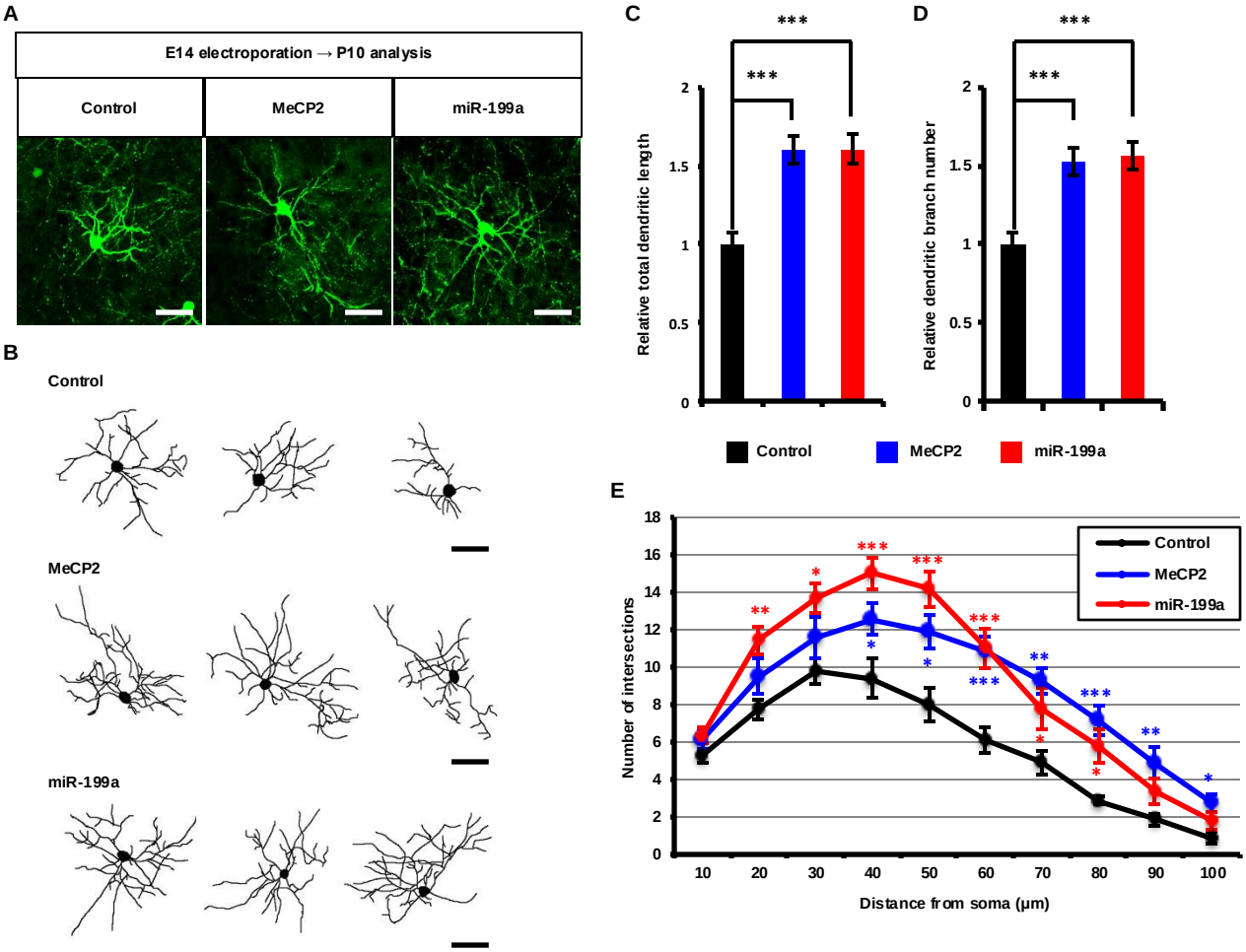

K. Irie et al. Fig. 6

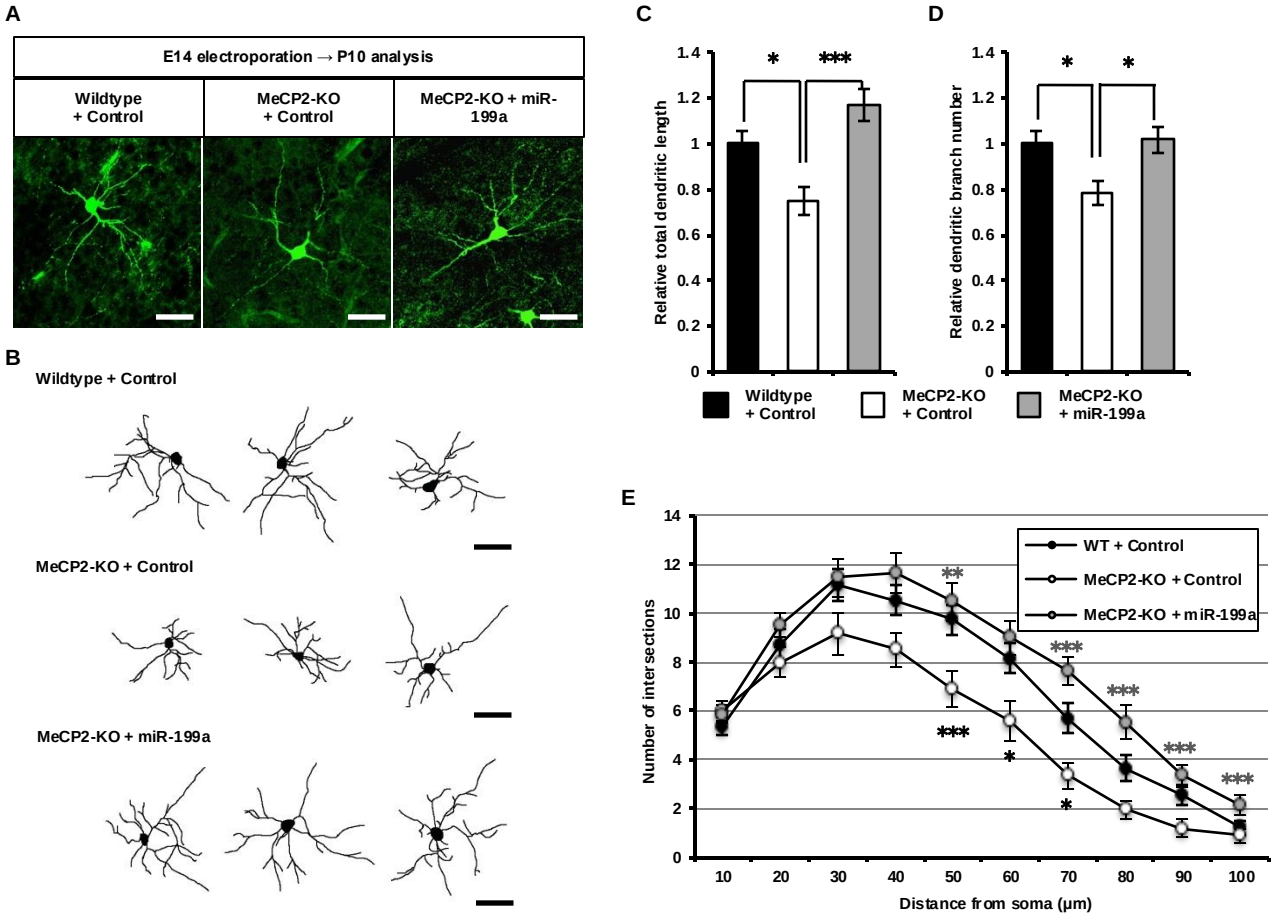

K. Irie et al. Fig. 7

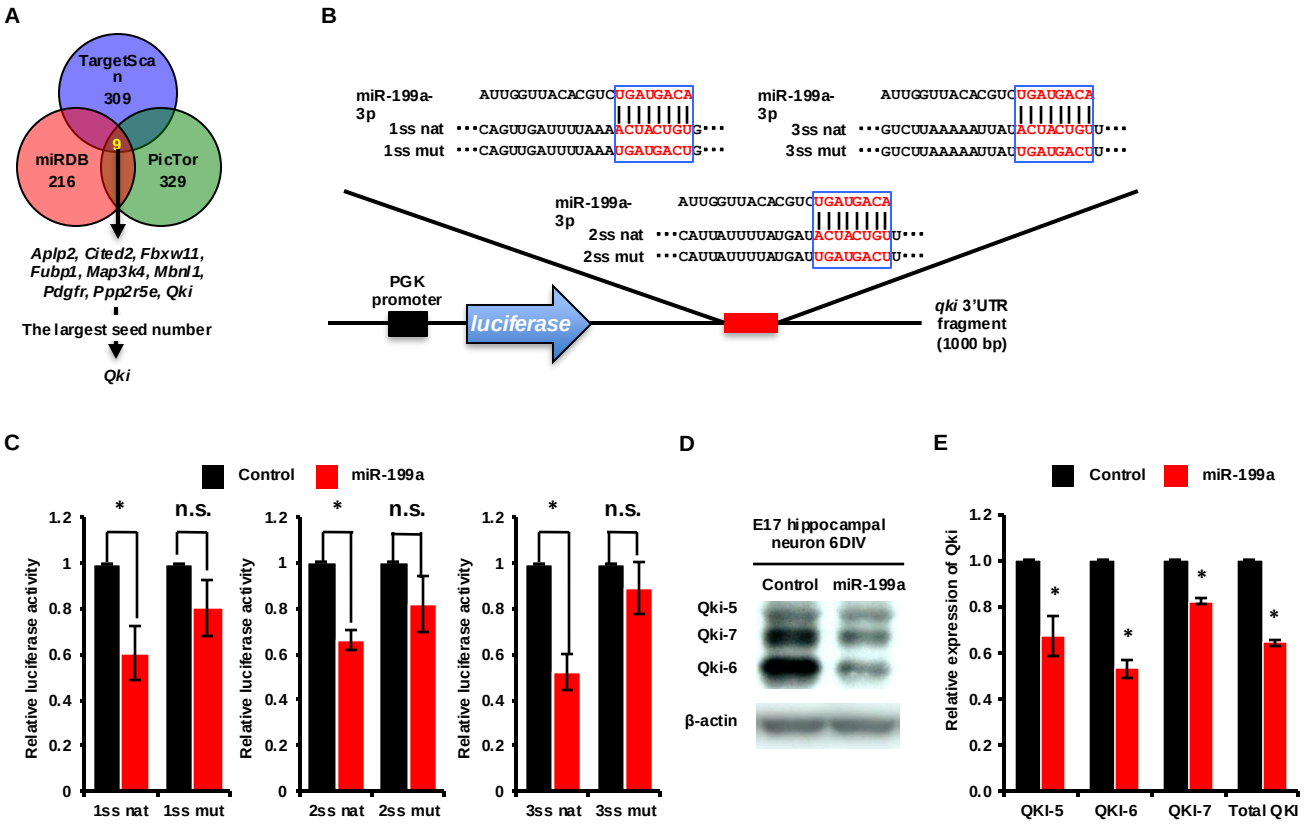
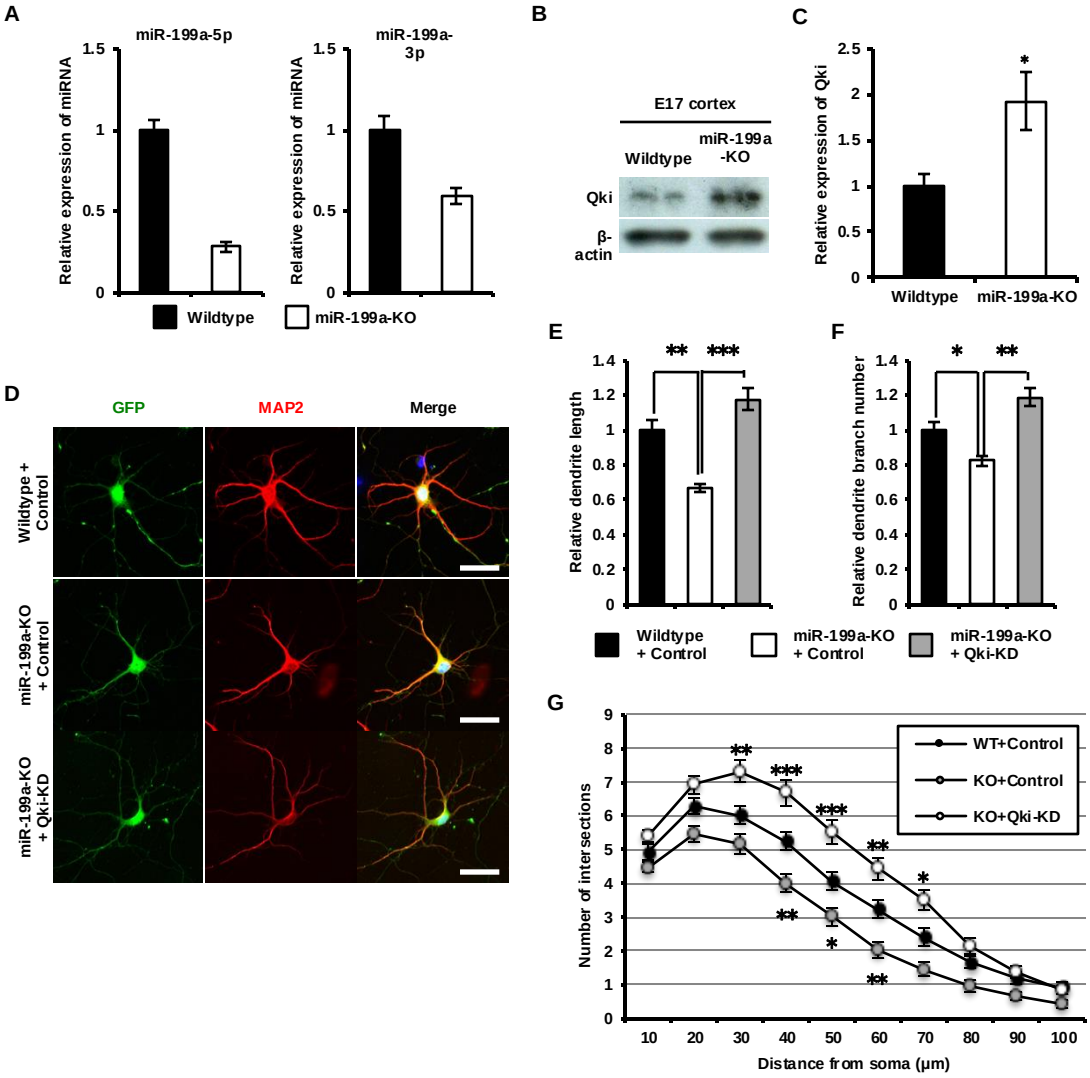
K. Irie et al. Fig. 8